Journal of Medicinal Chemistry

ARTICLE

pubs.acs.org/jmc

# Gd Complexes of Macrocyclic Diethylenetriaminepentaacetic Acid (DTPA) Biphenyl-2,2′-bisamides as Strong Blood-Pool Magnetic Resonance Imaging Contrast Agents

Ki-Hye Jung,[†] Hee-Kyung Kim,[‡] Gang Ho Lee,[§] Duk-Sik Kang,[∥] Ji-Ae Park,[⊥] Kyeong Min Kim,[⊥] Yongmin Chang,*[,‡,∥] and Tae-Jeong Kim*[,†]

[†]Department of Applied Chemistry, [‡]Department of Medical and Biological Engineering, and [§]Department of Chemistry, Kyungpook National University, University Road 80, Daegu, 702-701, Republic of Korea

[∥]Department of Diagnostic Radiology and Molecular Medicine, Kyungpook National University, Dongin-dong 2-ga, Daegu, 700-422, Republic of Korea

[⊥]Laboratory of Nuclear Medicine Research, Molecular Imaging Research Center, Korea Institute of Radiological Medical Science, Nowon-gil 75, Seoul, 139-706, Republic of Korea

Supporting Information

**ABSTRACT:** We report the synthesis of macrocyclic DTPA conjugates of 2,2′-diaminobiphenyl and their Gd complexes of the type $[Gd(\mathbf{L})(H_2O)]\cdot xH_2O$ (**2a**,**b**; **L** = **1a**,**b**) for use as new MRI blood-pool contrast agents (MRI BPCAs). Pharmacokinetic inertness of **2** compares well with those of analogous Gd-DTPA MRI CAs currently in use. The present system also shows very high stability in human serum. The $R_1$ relaxivity reaches 10.9 $mM^{-1}$ $s^{-1}$, which is approximately 3 times as high as that of structurally related Gd-DOTA ($R_1$ = 3.7 $mM^{-1}$ $s^{-1}$). The $R_1$ relaxivity in HSA goes up to 37.2 $mM^{-1}$ $s^{-1}$, which is almost twice as high as that of MS-325, a leading BPCA, demonstrating a strong blood pool effect. The in vivo MR images of mice obtained with **2b** are coherent, showing strong signal enhancement in heart, abdominal aorta, and small vessels. Even the brain tumor is vividly enhanced for an extended period of time. The structural uniqueness of **2** is that it is neutral in charge and thus makes no resort to electrostatic interaction, supposedly one of the essential factors for the blood-pool effect.

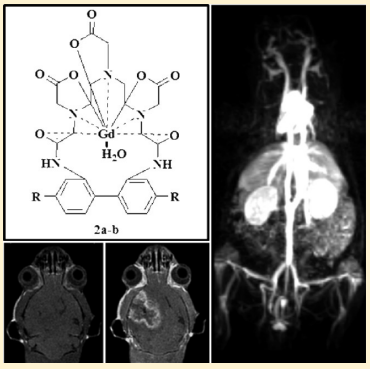


## INTRODUCTION

Magnetic resonance imaging (MRI) is a powerful, noninvasive diagnostic technique of the human anatomy, physiology, and pathophysiology on the basis of superior spatial resolution and contrast useful in providing anatomical and functional images of the human body.[1] At present, a large number of MRI techniques are performed employing Gd(III) complexes to enhance the image contrast by increasing the water proton relaxation rate in the body.[2] Some representative advantages of employing the Gd(III) ion come from their unique properties such as (i) seven unpaired electrons, (ii) nine coordination sites, and (iii) suitable electronic relaxation time. Despite their wide and successful applications in clinics, however, conventional Gd(III)-based low-molecular-weight CAs are mostly extracellular fluid (ECF) agents exhibiting rapid extravasation from the vascular space. As a result, the time window for imaging is considerably reduced, thus limiting acquisition of high-resolution images.[3−5]

In order to overcome such limitations inherent to ECF CAs, the necessity for the development of BPCAs has risen in the expectation that they reside in the blood vessel for an extended period of time and thus are eliminated much more slowly from the circulation than their ECF counterparts. The BPCAs provide strong and prolonged vascular enhancement. The BPCAs thus far developed may be divided into three classes according to their mechanism of action: (i) the noncovalent binding of low-molecular Gd chelates (GdL) to HSA to prevent immediate leakage into the interstitial space;[6−8] (ii) systems incorporating polymers or liposomes based on an increase in the size of CAs, which slows leakage through endothelial pores;[9−12] (iii) systems based on nanoparticles, involving a change in the route of elimination.[13−15] The most successful approach so far is the class i represented by MS-325, a Gd−DTPA derivative containing a cholic acid moiety. These complexes bind strongly and reversibly to HSA, leading to not only high relaxivity at clinical field strengths but also much longer residence time in the blood compared to ECF agents. The lipophilic component represented by aromatic moieties in the chelate is responsible for the generation of noncovalent interactions between the corresponding Gd chelate and HSA.[16,17] The anionic phosphodiester moiety in MS-325 is also known to contribute in a synergistic manner to the noncovalent binding interaction with HSA. Yet, since anionic Gd complexes lead to

**Received:** February 23, 2011
**Published:** June 27, 2011

**Scheme 1. Synthesis of 1and 2**

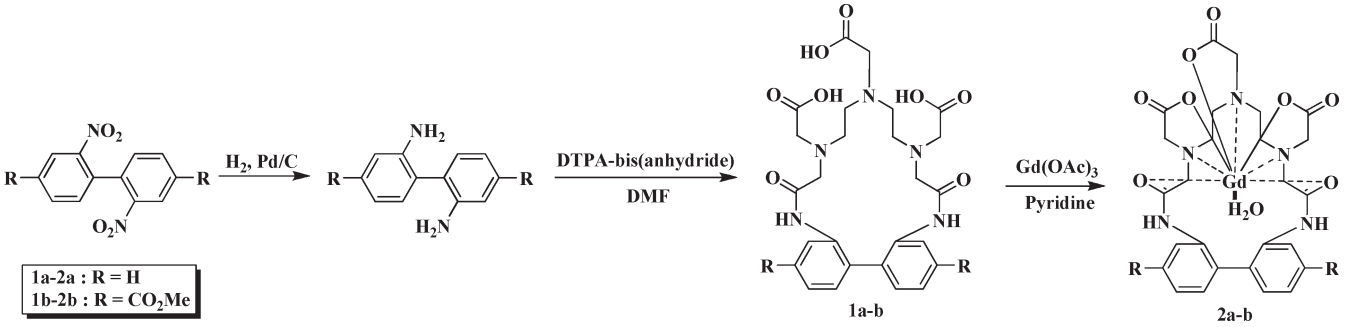


high osmolality under physiological conditions giving rise to some adverse effects, efforts have focused on the preparation of neutral analogues based on the Gd macrocycle with the concomitant aim to achieve thermodynamic stability as well as kinetic inertness.[2,9−12]

In line with these efforts and as part of our continued search for Gd-based MRI BPCAs,[18] we have designed and synthesized macrocyclic DTPA-(biphenyl-2,2′-bisamide) (**1a,b**, Scheme 1) for use as a ligand leading to the formation of MRI BPCA belonging to class i. Our justification for their synthesis may come from the expectation that **1** would form a neutral, macrocyclic Gd(III) complex $[Gd(\mathbf{1})(H_2O)]\cdot xH_2O$ (Scheme 1) carrying a highly liphophilic biphenyl on the chelate backbone.

## EXPERIMENTAL SECTION

**General Remarks.** All reactions were carried out under an atmosphere of dinitrogen using the standard Schlenk techniques. Solvents were purified and dried using standard procedures. DTPA was obtained from TCI and used without further purification. The *N,N*-bis(anhydride) of DTPA was prepared according to the literature methods.[19] All other commercial reagents were purchased from Aldrich and used as received unless otherwise stated. Deionized water was used for all experiments. The $^1$H NMR experiment was performed on a Bruker Advance 400 spectrometer by Center for Instrumental Analysis, Kyungpook National University (KNU). Chemical shifts are given as $\delta$ values with reference to tetramethylsilane (TMS) as the internal standard. Coupling constants are in Hz. Elemental analyses were performed by Center for Instrumental Analysis, KNU, and Catholic University in Daegu. FAB mass spectra were obtained by using a JMS-700 model (Jeol, Japan) mass spectrophotometer by Korea Basic Science Institute (KBSI). The purity of all products was determined to be above 95% by elemental analysis.

**Synthesis. 2,2′-Diaminobiphenyl.** To a solution of 2,2′-dinitrobiphenyl (5.0 g, 20.5 mmol) in ethyl acetate (90 mL) in an autoclave was added Pd/C (10%, 2.0 g). The reaction vessel was flushed several times and pressurized with dihydrogen to 700 kPa. The vessel was sealed and the mixture stirred at room temperature for 18 h, after which the pressure was released and the catalyst separated by filtration with ethyl acetate (3 × 10 mL). The solvent was removed under reduced pressure and the residue recrystallized from hexane/chloroform to give pale violet crystals. Yield: 3.5 g (94%). $^1$H NMR ($CDCl_3$): $\delta$ = 7.19−7.15 (t, 2H, 4,4′-*H*), 7.12−7.10 (d, 2H, 6,6′-*H*), 6.84−6.80 (t, 2H, 5,5′-*H*), 6.78−6.75 (d, 2H, 3,3′-*H*), 3.68 (s, 4H, $-NH_2$). $^{13}$C NMR ($CDCl_3$): $\delta$ = 144.5 (2,2′-C), 131.5 (4,4′-C), 129.2(6,6′-C), 125.1 (5,5′-C), 119.3(1,1′-C), 116.1(3,3′-C). Anal. Calcd for $C_{12}H_{12}N_2$: C, 78.23; H, 6.57; N, 15.21. Found: C, 77.92; H, 6.53; N, 15.12.

**Dimethyl 2,2′-Dinitrobiphenyl-4,4′-dicarboxylate.** The title compound was prepared according to the literature methods.[20] The crude product thus obtained was further purified by chromatography ($SiO_2$, hexane/ethyl acetate 75:25) to give a yellow crystalline solid after usual workups. Yield: 3.2 g (77%). $^1$H NMR ($CDCl_3$): $\delta$ = 8.90 (s, 2H, 3,3′-*H*), 8.35 (d, 2H, 5,5′-*H*), 7.40−7.38 (d, 2H, 6,6′-*H*), 4.02 (s, 6H, $-COOCH_3$). $^{13}$C NMR ($CDCl_3$): $\delta$ = 164.5 ($-COOCH_3$), 146.8 (2,2′-C), 137.7 (1,1′-C), 134.3 (5,5′-C), 131.8 (4,4′-C), 131.0 (6,6′-C), 126.0 (3,3′-C), 53.0 ($-COOCH_3$). Anal. Calcd for $C_{16}H_{12}N_2O_8$: C, 53.34; H, 3.36; N, 7.78. Found: C, 53.47; H, 3.34; N, 7.77.

**Dimethyl 2,2′-Diaminobiphenyl-4,4′-dicarboxylate.** To a solution of dimethyl 2,2′-dinitrobiphenyl-4,4′-dicarboxylate (3.0 g, 8.3 mmol) in acetic acid (60 mL) in an autoclave was added Pd/C (10%, 1.5 g). The reaction vessel was flushed several times and pressurized with dihydrogen to 700 kPa. The vessel was sealed and the mixture stirred at 30 °C overnight, after which the pressure was released and the catalyst separated by filtration with acetic acid (3 × 5 mL). The solvent was removed under reduced pressure and the residue purified by chromatography ($SiO_2$, hexane/ethyl acetate 6:4) to give a yellow crystalline solid. Yield: 2.3 g (91%). $^1$H NMR ($CDCl_3$): $\delta$ = 7.51−7.50 (d, 2H, 5,5′-*H*), 7.47 (d, 2H, 6,6′-*H*), 7.19−7.17 (s, 2H, 3,3′-*H*), 3.92 (s, 6H, $-COOCH_3$), 3.83 (br, 4H, $NH_2-$). $^{13}$C NMR ($CDCl_3$): $\delta$ = 167.0 ($-COOCH_3$), 146.0 (2,2′-C), 131.2 (4,4′-C), 130.0 (6,6′-C), 128.0 (1,1′-C), 117.6 (5,5′-C), 116.2 (3,3′-C), 52.3 ($-COOCH_3$). Anal. Calcd for $C_{16}H_{16}N_2O_4$: C, 63.99; H, 5.37; N, 9.33. Found: C, 63.85; H, 5.42; N, 9.24.

**1a.** To a stirred solution of 2,2′-diaminobiphenyl (0.8 g, 4.4 mmol) in DMF (10 mL) was added DTPA-bis(anhydride) (1.6 g, 4.4 mmol) in DMF (5 mL) in one portion. The mixture was stirred at 70 °C for 16 h, after which the solvent was removed under reduced pressure. The solid residue was taken up in methanol (5 mL) and filtered through a short silica gel column to remove any solid impurities and ether added to precipitate out a white solid. This was isolated by filtration and dried under vacuum to give the desired product as a white powder. Yield: 1.9 g (81%). $^1$H NMR ($CDCl_3$): $\delta$ = 7.52−7.50 (d, 2H, 3,3′-*H*), 7.46−7.45 (d, 2H, 6,6′-*H*), 7.37−7.35 (t, 2H, 4,4′-*H*), 7.22 (t, 2H, 5,5′-*H*), 3.43−3.38 (m, 10H, $-NHCOCH_2$ and $-NCH_2COO$), 3.28−3.09 (m, 8H, $-NCH_2CH_2N$). Anal. Calcd for $C_{26}H_{31}N_5O_8\cdot 1H_2O$: C, 55.87; H, 5.94; N, 12.52. Found: C, 55.27; H, 5.96; N, 12.53. FAB-MS (*m*/*z*): calcd for $C_{26}H_{32}N_5O_8$, 542.22 ($[MH]^+$). Found: 542.41.

**1b.** The title compound was prepared as described above for the preparation of **1a** by replacing 2,2′-diaminobiphenyl with dimethyl 2,2′-diaminobiphenyl-4,4′-dicarboxylate (0.8 g, 2.7 mmol) in DMF (10 mL). The product was obtained as an off-white powder. Yield: 1.3 g (76%). $^1$H NMR (DMSO): $\delta$ = 9.83 (br, 3H, $-COOH$), 8.14 (s, 2H, 3,3′-*H*), 7.89−7.86 (d, 2H, 5,5′-*H*), 7.41−7.39 (d, 2H, 6,6′-*H*), 3.87 (s, 6H, $-COOCH_3$), 3.24−3.07 (m, 10H, $-NHCOCH_2$ and $-NCH_2COO$), 2.91−2.87 (m, 8H, $-NCH_2CH_2N$). Anal. Calcd for $C_{30}H_{35}N_5O_{12}$: C, 54.79; H, 5.36; N, 10.65. Found: C, 54.06; H, 5.43; N, 10.64. FAB-MS (*m*/*z*): calcd for $C_{30}H_{36}N_5O_{12}$, 658.24 ($[MH]^+$). Found: 658.23 ($[MH]^+$).


dx.doi.org/10.1021/jm2002052 |*J. Med. Chem.* 2011, 54, 5385–5394

**Typical Procedure for the Preparation of 2.** To a solution of **1** (1.5 mmol) in pyridine (7 mL) was added an equivalent amount of $Gd(OAc)_3$ (1.5 mmol). The suspension was stirred overnight at 70 °C during which time the solution became homogeneous. The solvent was removed and the residue dissolved in a minimum amount of ethanol to be passed through Celite to remove any solid impurities. Ether was added to the filtrate to precipitate an off-white powder which was dried in vacuo. **2a**. Yield: 0.9 g (91%). Anal. Calcd for $C_{26}H_{28}GdN_5O_8 \cdot 4H_2O$: C, 40.67; H, 4.73; N, 9.12. Found: C, 40.79; H, 4.95; N, 9.29. FAB-MS ($m/z$): calcd for $C_{26}H_{28}GdN_5NaO_8$, 719.11 ($[MNa]^+$). Found; 719.54. **2b**. Yield: 1.1 g (88%). Anal. Calcd for $C_{30}H_{32}GdN_5O_{12} \cdot 4H_2O$: C, 40.76; H, 4.56; N, 7.92. Found: C, 40.01; H, 4.37; N, 7.97. FAB-MS ($m/z$): calcd for $C_{30}H_{33}GdN_5O_{12}$, 812.13 ($[MH]^+$). Found: 812.12 ($[MH]^+$).

**[Dy(1)($H_2O$)] (3).** The title compound was prepared as described above for the preparation of **2** by replacing $Gd(OAc)_3$ with $DyCl_3$. The product was obtained as an off-white powder. **3a**. Yield: 1.4 g (80%). FAB-MS ($m/z$): calcd for $C_{26}H_{28}DyN_5NaO_8 \cdot H_2O$, 721.24 ($[MH]^+$). Found; 721.16 ($[MH]^+$). **3b**. Yield: 1.7 g (89%). FAB-MS ($m/z$): calcd for $C_{30}H_{33}DyN_5O_{12} \cdot H_2O$, 837.15 ($[MH]^+$). Found: 837.28 ($[MH]^+$).

**Transmetalation Kinetics.** This experiment was performed according to the literature method, where the water proton relaxation rates ($R_1^P$) of buffered solutions (phosphate buffer, pH 7.4) containing equimolar amounts of **2** (2.5 mM) and $ZnCl_2$ (2.5 mM) are measured.[21] Namely, to a buffered solution of **2** (1 mL) was added a buffered solution of $ZnCl_2$ (10 $\mu$L). The mixture was vigorously stirred and 300 $\mu$L of the solution taken up for the relaxometric study. Control studies have also been carried out with Gd-DTPA-BMA, Gd-DOTA, Gd-EOB-DTPA, and Gd-BOPTA for comparative purposes. The $R_1^P$ relaxation rate was obtained after subtraction of the diamagnetic contribution of the proton water relaxation from the observed relaxation rate $R_1 = (1/T_1)$. The measurements were performed on a 3 T whole body system (Magnetom Tim Trio, Siemens, Germany) at room temperature.

**Determination of Kinetic Constants.** These constants were fitted according to eqs 1−4.

$$GdL + Zn^{2+} \underset{k_r}{\overset{k_f}{\rightleftarrows}} Gd^{3+} + [ZnL]^{1-} \quad (1)$$

where $k_f$ and $k_r$ are the rate constants for the forward and reverse transmetalation reactions, respectively. The rate of transmetalation can be written as in eq 2. Here $[ZnL] = [GdL]_0 - [GdL]$, with $[GdL]_0$ being the initial concentration of the gadolinium complex.

$$\frac{d[GdL]}{dt} = -k_f'[GdL] + k_r'[ZnL] \quad (2)$$

The concentration of GdL at time $t$ can be written as in eq 3.

$$[GdL] = [GdL]_\infty + ([GdL]_0 - [GdL]_\infty)\, e^{k_1 t} \quad (3)$$

$k_1 = k'_f + k'_r$, and $[GdL]_\infty$ is the equilibrium concentration of GdL. Thus, $k_f$ can be calculated as

$$k_f' = k_1 \frac{[GdL]_0 - [GdL]_\infty}{[GdL]_0} \quad (4)$$

The $k'_f$ is obtainable by nonlinear curve fitting of transmetalation data using MATLAB R2008a in eq 4.

**Dy(III)-Induced Water $^{17}O$ Shifts.** **3** was dissolved in water containing 20% $D_2O$ and 5% $^{17}O$-enriched water (Isotech, U.S.). The pH of the solution was adjusted to the physiological value (pH 7.0). The dysprosium-induced shift measurements were performed at a Dy(III)/ligand molar ratio corresponding to the desired complex stoichiometry by varying the concentration of **3** over the range 20−80 mmol $dm^{-3}$. $^{17}O$ NMR experiments were run at 500 MHz using a Varian Unity INOVA instrument (11.8T, 67.814 MHz) at room temperature. Samples were sealed in glass spheres, fitting into 10 nm NMR tubes in order to eliminate susceptibility correction to the chemical shift. The hydration numbers in **3** were fitted using eq 5[22]

$$\Delta\delta = q\Delta[Dy(ligand)_n(H_2O)_q]/[H_2O] \quad (5)$$

The slope of a plot of the Dy(III)-induced shift versus the Dy(III) concentration is proportional to the hydration number in the complex. The hydration number is obtained by linear fitting of the dysprosium-induced shift data using OriginPro 8.

**Relaxivity.** $T_1$ measurements were carried out using an inversion recovery method with a variable inversion time (TI) at 1.5 T (64 MHz, GE Healthcare, Milwaukee, WI, U.S.). The magnetic resonance (MR) images were acquired at 35 different TI values ranging from 50 to 1750 ms. $T_1$ relaxation times were obtained from the nonlinear least-squares fit of the signal intensity measured at each TI value. For $T_2$ measurements the CPMG (Carr−Purcell−Meiboon−Gill) pulse sequence was adapted for multiple spin−echo measurements. Thirty-four images were acquired with 34 different echo time (TE) values ranging from 10 to 1900 ms. $T_2$ relaxation times were obtained from the nonlinear least-squares fit of the mean pixel values for the multiple spin−echo measurements at each echo time. Relaxivities ($R_1$ and $R_2$) were then calculated as an inverse of the relaxation time per mM. The determined relaxation times ($T_1$ and $T_2$) and relaxivities ($R_1$ and $R_2$) are finally image-processed to give the relaxation time map and relaxivity map, respectively.

**Brain Tumor Model.** The C6 glioma cells were grown in a monolayer with Dulbecco's modified Eagle medium (DMEM), supplemented with fetal calf serum (10%), L-glutamine (2%), penicillin/streptomycin (0.2%) and incubated at 37 °C in a mixture of air/$CO_2$ (95%/5%). Cells were suspended in an agar solution (1%) prepared with supplemented DMEM ($10^6$ cell $mL^{-1}$) shortly before injection and injected with 10 $\mu$L of the mixture. Agarose was used to prevent the cells from spreading out of the injection site. The rats (40−60 g of body weight) were anesthetized (1.5% isoflurane in oxygen) and placed on a stereotactic head holder. A middle scalp incision was made. The cell suspension (10 $\mu$L) was slowly injected for 10 min using a Hamilton syringe (1.0 mm diameter). The syringe was slowly removed 2−5 min after cell injection, and the scalp was sutured. The MR experiments were carried out 6 or 7 weeks after tumor cell implantation.[23]

**Serum Stability Assay.** The serum stability assay was performed in two ways. The first method involves traditional HPLC monitoring of the signal intensity of the Gd complex in human serum from the UV absorbance detector at 240 nm for the present studies.[24,25] The HPLC system (high pressure liquid chromatography, KNAUER, Berlin, Germany) equipped with a Develosil ODS-HG-5 column (6.0 mm × 250 mm; Nomura Chemical Co., Ltd., Aichi, Japan) was used for the measurement. Elution conditions were as follows: A mixture of an aqueous solution of TFA (0.1%, v/v) and an acetonitrile solution of TFA (0.1%, v/v) with a 30 min linear gradient (from 5% to 80%) at a flow rate of 1.7 mL/min was used. Samples were prepared as follows: **2b** (0.2 mg) was dissolved initially in DMSO (20 $\mu$L) to be diluted with water (80 $\mu$L). The solution was divided into two vials: the first solution (60 $\mu$L) was added to human serum (940 $\mu$L) in a 2 mL vial for the purpose of incubation at 37 °C, and the second one (30 $\mu$L) was diluted with water (470 $\mu$L) in a 1 mL vial as a standard. Aliquots (60 $\mu$L each) of the first solution were analyzed without dilution at different time points. In addition, a standard serum solution was prepared by mixing DMSO (12 $\mu$L), water (48 $\mu$L), and human serum (940 $\mu$L). The second method was developed by us and involves the determination of $Gd^{3+}$ concentration by measuring the ratio of relaxivities, $R_1^P(t)/R_1^P(0)$, as a function of incubation time for the serum solution of **2**.[18b] This method, although qualitative, is a handy and simple replacement of the traditional HPLC method. The typical procedure is as follows: To a solution of aqueous human serum (Innovative Research) (180 $\mu$L) was added an aqueous

solution of **2** (20 $\mu$L, 5 mM) at 4 °C. The mixture was incubated at 37 °C at different intervals (0 min, 30 min, 1 h, 2 h, 4 h, 48 h, and 96 h), after which time aqueous TCA (20%, 100 $\mu$L) was added to precipitate free human serum. The supernatant solution, after removal of the white precipitates of human serum by centrifugation at 4 °C for 10 min, was taken for relaxivity measurement at a 3 T whole body system at room temperature. In this way the serum stability assay can be qualitatively accomplished, since any changes in $R_1$ relaxivities (an increase, in fact) of the solutions prepared before and after incubation would indicate the release of free Gd(III) ion from **2**.

**In Vitro Cell Toxicity.** The CT-26 mouse colon carcinoma cell line was purchased from the American Type Culture Collection (ATCC, Rockville, MD). Cells were maintained in DMEM (Welgene), supplemented with 10% FBS and 1% antibiotic (all purchased from Gibco). The medium was replaced every 2 days, and CT-26 cells were placed into a 96-well plate ($2 \times 10^3$ cells/well per 50 $\mu$L). Magnevist Gd complexes were added to each well (1 nM to 1 mM per 50 $\mu$L). After incubation for 5 days at 37 °C in a 5% $CO_2$ atmosphere, 3-(4,5-dimethylthiazol-2-yl)-5-(3-carboxymethoxyphenyl)-2-(4-sulfophenyl)-2*H*-tetrazolium, inner salt (MTS, Promega, Madison, WI) was added to each well (20 $\mu$L/well). After an additional 1 h of incubation, proliferation of the treated cells was quantified by measuring the absorbance of the culture medium at 492 nm with a 96-well plate reader (GENios, TECAN Co., Boston, MA). The cytotoxicities were compared. IMR-90 human embryonic lung fibroblasts were also employed. Cells were maintained in DMEM (Gibco) supplemented with heat-inactivated FCS (10%), penicillin (100 IU/mL), streptomycin (100 mg/mL), and gentamicin (200 mg/mL) (all purchased from Gibco). The medium was replaced every 2 days, and cells placed into a 96-well plate ($1 \times 10^4$ cells/well per 200 $\mu$L). Various Gd(III) concentrations (IMR-90: 1 nM to 0.1 mM) of the contrast agent were added into the culture serum free medium and incubated for 24 h. CCK-8 (10 $\mu$L) was then added to each well to evaluate cell viability. The solution was removed after 4 h at 37 °C. The OD (optical density) was read at 450 nm using a microplate reader (Molecular Device, USA Bio-Rad 550 reader) to determine the cell viability/toxicity.

**In Vivo MR Imaging.** All animal experiments were performed in accordance with the rules of the animal research committee of Kyungpook National University. Six-week-old male ICR (Institute of Cancer Research) mice with weights of 29−31 g were used for the MRI. Eight-week-old male SD (Sprague−Dawley) rats with weights of 100−120 g were used for the brain tumor MR imaging. Ten-week-old male SD rats with weights of 350−400 g were used for the CE-MRA. The mice ($n$ = 4) and rats ($n$ = 8) were anesthetized with 1.5% isoflurane in oxygen. Measurements were made before and after injection of **2b** via tail vein. The amount of CA per each injection is 0.1 mmol [Gd]/kg for MR and CE-MRA images. After each measurement the mouse was revived from anesthesia and placed in the cage with free access to food and water. During these measurements, the animals were maintained at approximately 37 °C using a warm water blanket. Whole body MR images were taken with a 1.5 T MR unit (GE Healthcare, Milwaukee, WI, U.S.) equipped with a homemade small animal rf coil. The coil was of the receiver type with its inner diameter being 50 mm. The imaging parameters for 3D fast SPGR (spoiled GRASS images) are as follows: repetition time (TR) = 9.2 ms; echo time (TE) = 2.1 ms; 12 mm field of view (FOV); 256 × 192 matrix size; 0.8 mm slice thickness; number of acquisitions (NEX) = 8. Images were obtained for 110 min after injection. Brain tumor MR images were taken with a 3 T MR unit (GE Healthcare, Milwaukee, WI, U.S.) equipped with a homemade small animal rf coil. The imaging parameters for SE (spin echo) are as follows: repetition time (TR) = 550 ms; echo time (TE) = 11 ms; 4 mm field of view (FOV); 128 × 128 matrix size; 0.8 mm slice thickness; number of acquisitions (NEX) = 4. CE-MRA was carried out with a 3.0 T MR unit (Magnetom Tim Trio, Siemens Medical Solution, Erlangen, Germany) equipped with 8HR wrist coil. The imaging parameters for CE-MRA vibe are as follows: repetition time (TR) = 3.3 ms; echo time (TE) = 1.3 ms; 17 mm field of view (FOV); 0.9 mm slice thickness; 192 × 65 matrix size; number of acquisitions (NEX) = 1. Each image was taken at an interval of 11 s.

**Table 1. Kinetic Constants of 2, Gd Ferromide, Gd-DOTA, Gd-EOB-DTPA, Gd-BOPTA, and Gd-DTPA-BMA**

| complex | $K_1$ ($min^{-1}$) | $[Lig\ Gd]_\infty$ (mol/L) | $K'_f$ ($min^{-1}$) |
|---|---|---|---|
| **2a** | $1.11 \times 10^{-3}$ | $1.19 \times 10^{-3}$ | $5.79 \times 10^{-4}$ |
| **2b** | $1.04 \times 10^{-3}$ | $1.26 \times 10^{-3}$ | $5.15 \times 10^{-4}$ |
| Gd ferromide[a] | $1.19 \times 10^{-3}$ | $1.35 \times 10^{-3}$ | $5.46 \times 10^{-4}$ |
| Gd-DOTA[a] | $1.81 \times 10^{-4}$ | $1.53 \times 10^{-3}$ | $0.69 \times 10^{-4}$ |
| Gd-EOB-DPTA | $1.39 \times 10^{-3}$ | $1.37 \times 10^{-3}$ | $6.25 \times 10^{-4}$ |
| Gd-BOPTA[a] | $1.65 \times 10^{-3}$ | $1.24 \times 10^{-3}$ | $8.32 \times 10^{-4}$ |
| Gd-DTPA-BMA[a] | $1.41 \times 10^{-3}$ | $1.09 \times 10^{-3}$ | $7.96 \times 10^{-4}$ |

[a] Data obtained from ref 18b.

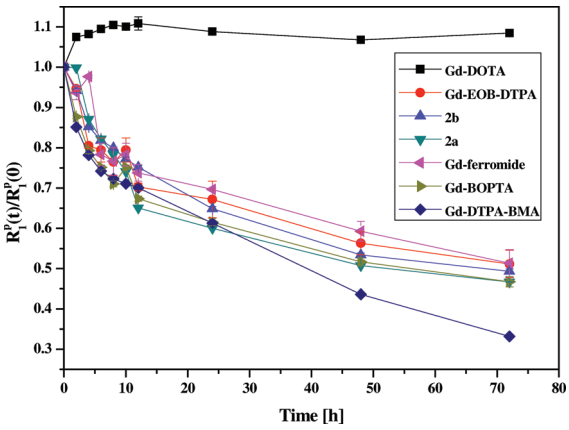


**Figure 1.** Evolution of $R_1^P(t)/R_1^P(0)$ as a function of time for various MRI CAs.

**Image Analysis.** The anatomical locations with enhanced contrast were identified with respect to heart, kidney, and liver on postcontrast MR images. For quantitative measurement, signal intensities in specific regions of interest (ROI) were measured using Advantage Window software (GE Medical, U.S.). The CNR (contrast to noise ratio) was calculated using eq 6, where SNR is the signal-to-noise ratio.

$$CNR = SNR_{post} - SNR_{pre} \quad (6)$$

## RESULTS AND DISCUSSION

**Synthesis and Characterization.** Scheme 1 shows the preparation of **1** and **2**. The scheme initially requires the preparation of 2,2′-diaminobiphenyls by catalytic hydrogenation of the corresponding 2,2′-dinitrobiphenyls. Subsequent condensation with DTPA-bis(anhydride) resulted in the formation of **1** as macrocyclic DTPA-bis(amide) chelates anchored by biphenyl. It is noted here that the condensation proceeded to form a macrocyclic chelate rather than linear, oligomeric analogues. The macrocyclization such as that observed here has a precedent with 1,1′-ferrocenediyldiamines which on reaction with DTPA-bis(anhydride) led to the formation of analogous macrocyclic DTPA-bis(amides).[18b] These ligands form Gd(III) complexes of the type $[Gd(\mathbf{L})(H_2O)]\cdot xH_2O$ (**2a,b**; **L** = **1a,b**) by simple complexation with an equimolar amount of $Gd(OAc)_3$ in pyridine. All complexes were isolated as off-white, hygroscopic solids by repeated precipitation with cold diethyl ether from the reaction mixture. The formation of **1** and **2** was confirmed by microanalysis and


dx.doi.org/10.1021/jm2002052 |J. Med. Chem. 2011, 54, 5385–5394

spectroscopic techniques such as $^{1}H$ and $^{13}C$ NMR, HRFAB mass spectrometry. For instance, **2a** and **2b** exhibit $[MNa]^+$ and $[MH]^+$ signals at $m/z$ of 719.54 and 812.12, respectively. Although ligands are insoluble in water, their Gd complexes exhibit fairly good water solubility (up to 0.25 M).

**Transmetalation Kinetics.** Protonation constants and thermodynamic stability constants could not be obtained because of water insolubility of ligands. Yet transmetalation kinetic data would be sufficient enough to provide relevant information about the stability of Gd complexes under physiological conditions. The Gd chelates, although they are thermodynamically stable, may be kinetically labile enough to undergo transmetalation by endogenous ions. In such a process, the paramagnetic Gd(III) ion is expelled from the complex. Endogenous ions likely to compete with Gd(III) are Cu(II), Ca(II), and Zn(II).[26−28] The Cu(II) ion is present in very small concentrations in the blood (1−10 mol/L), whereas Ca(II) has relatively low affinity for acyclic ligands such as DTPA and DTPA-BMA (roughly 10 orders of magnitude lower than that of Gd(III)). Although the affinity for Ca(II) by cyclic ligand such as DOTA may be high enough, transmetalation by this ion can be ignored in the presence of other metal ions. For instance, only Zn(II) can displace a significant amount of Gd(III) because the concentration of the former in blood is relatively high (55−125 mol/L).[29] The stability of Gd complexes in the presence of Zn(II) is thus an important issue because transmetalation will induce a release of Gd(III) into the body and possible depletion of the endogenous ion subsequent to its elimination as a hydrophilic complex by the kidneys. If transmetalation of a soluble, paramagnetic Gd complex by diamagnetic Zn(II) ions were to occur in a phosphate-buffered solution, then the released Gd(III) would react to form $Gd_2(PO_4)_3$, the solubility of which is very low ($K_{sp} = 10^{-22.2}$ mol$^2$/L$^2$) and whose influence on the longitudinal relaxation rate of water is negligible.[30]

The relative value of $R_1^P$ at any time $t$, $R_1^P(t)/R_1^P(0)$, is therefore a good estimator of the extent of transmetalation. Its evolution over time gives relevant information about the kinetics of the reaction, whereas the plateau value theoretically reached at $t = \infty$ will reflect the thermodynamic aspects of the system.

Measurements were made of the buffered solutions (phosphate buffer, pH 7.4) containing equimolar amounts of **2** (2.5 mM) and $ZnCl_2$ (2.5 mM) as described in the Experimental Section,[21] and quantitative transmetalation kinetic data are provided in Table 1. Also provided are the data obtained with Gd-DTPA-BMA, Gd-DOTA, Gd-EOB-DTPA, and Gd-BOPTA for comparative purposes. The kinetic data are in good agreement with the semiquantitative results shown in Figure 1. The fitted graph of kinetic constants is provided in Figure S1 (ESI).

Quite obviously there must be a clear distinction in the evolution rate between complexes incorporating macrocyclic chelates and those containing acyclic ones.[18c] As such, Gd-DOTA reveals the highest kinetic stability (inertness), that is, the smallest $K'_{fj}$ as it possesses more five-membered metallacycles (eight in all) not alone with the macrocyclic motifs. On the other hand, complexes incorporating an acyclic ring such as

**Chart 1**

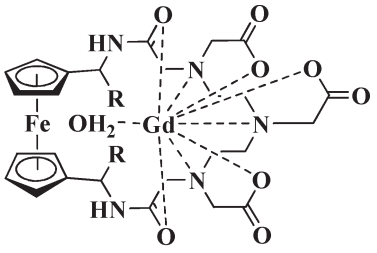


**Gd-ferromide: R = Me**

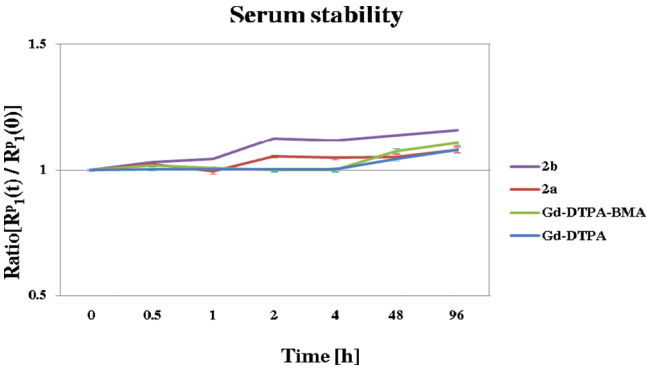


**Figure 2.** Human serum stability for **2**, Gd-DTPA-BMA, and Gd-DTPA.

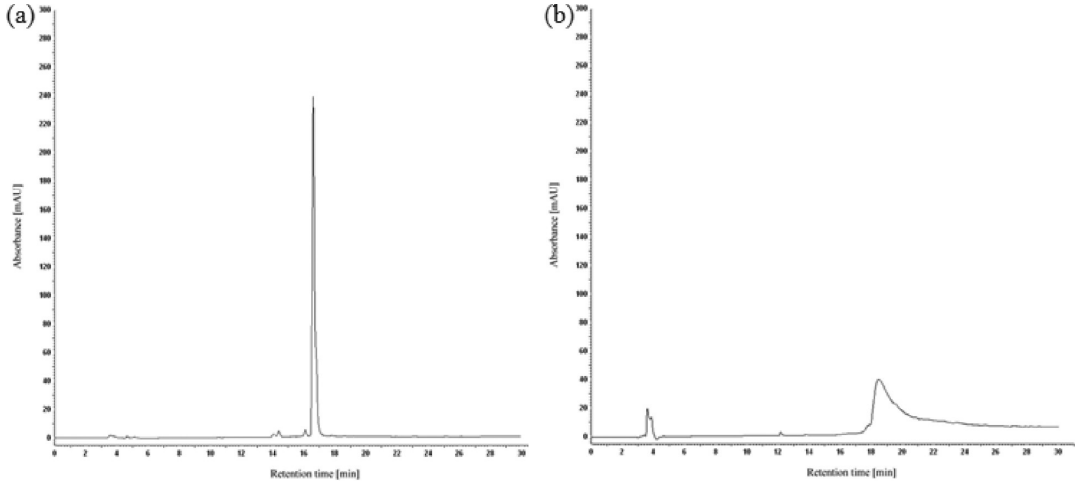


**Figure 3.** HPLC spectra of (a) **2b** and (b) human serum.


dx.doi.org/10.1021/jm2002052 |J. Med. Chem. 2011, 54, 5385–5394

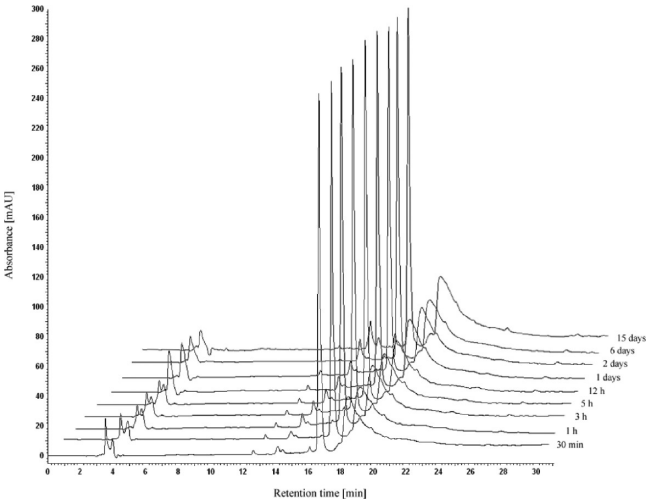


**Figure 4.** HPLC spectra of **2b** incubating in human serum at 37 °C at different time intervals.

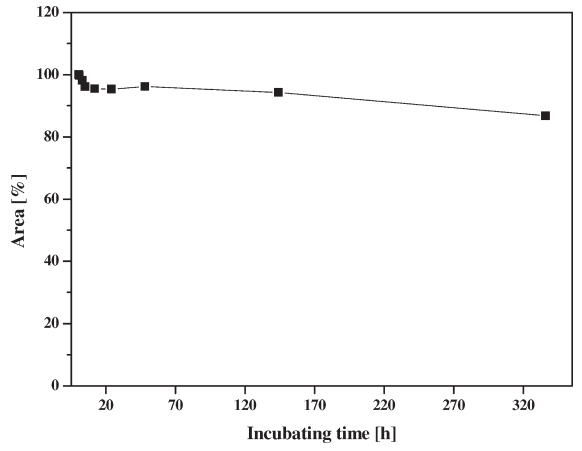


**Figure 5.** Quantitative results obtained by integration of area at $\tau$ = 17 min.

Gd-EOB-DTPA, Gd-BOPTA, and Gd-DTPA-BMA exhibit much lower kinetic stability with the $K'_f$ values being 7−12 times as high as that of Gd-DOTA. The kinetic stability of **2**, which also adopts a macrocycle and possesses fewer five-membered rings, is located between that of Gd-DOTA and Gd-DTPA as shown in Table 1 and Figure 1. It is informative to note that Gd ferromide (Chart 1), an organometallic analogue of macrocyclic DTPA-bis(amide), has a kinetic constant ($K'_f = 5.46 \times 10^{-4}$) quite close to that of **2**. All-in-all, a general trend, though qualitative, may be drawn as follows, in decreasing order of kinetic stability: Gd-DTPA ∼ Gd-DTPA-bis(amide) > macrocyclic Gd-DTPA-bis(amide) > Gd-DOTA.

**Serum Stability.** In addition to the kinetic stability of the present system, their biostability is equally essential for application in vivo. For this purpose we have developed a qualitative method of determining the $Gd^{3+}$ concentration by measuring the ratio of relaxivities, $R_1^P(t)/R_1^P(0)$, as a function of incubation time for the serum solution of **2**.[18b] Figure 2 shows serum stability assay performed on **2**, Gd-DTPA-BMA, and Gd-DTPA. The resulting proton longitudinal relaxation rate enhancement ($R_1^P$) thus essentially arises from the existence of solubilized and hydrated Gd(III)

**Table 2. Relaxivity Data of 2, Gd-DTPA, MS-325, Gd-EOB-DTPA, and Gd-BOPTA in Water and Blood (64 MHz, 310 K, 2 at 293 K)**

| | water | | blood (HSA, 0.67 mM) | | |
|---|---|---|---|---|---|
| | $R_1$, $mM^{-1}\,s^{-1}$ | $R_2$, $mM^{-1}\,s^{-1}$ | $R_1$, $mM^{-1}\,s^{-1}$ | $R_2$, $mM^{-1}\,s^{-1}$ | ratio $R_1/R_2$ |
| **2a** | 8.9 | 10.2 | 31.3 | 47.9 | 0.65 |
| **2b** | 10.9 | 13.5 | 37.2 | 62.8 | 0.59 |
| Gd-DTPA[a] | 3.3 | 3.9 | 4.3 | 4.4 | 0.97 |
| MS-325[a] | 5.2 | 5.9 | 19.0 | 37.0 | 0.51 |
| Gd-EOB-DTPA | 7.14 | 7.96 | 8.52 | 11.18 | 0.76 |
| Gd-BOPTA | 5.35 | 5.87 | 6.91 | 9.33 | 0.74 |

[a] Data obtained from ref 33.

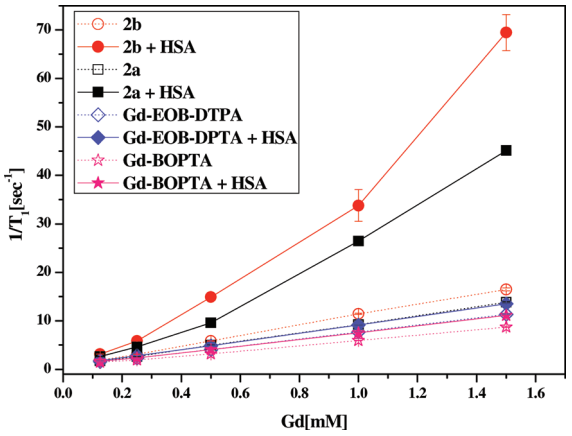


**Figure 6.** Plots of $R_1$ relaxivity of various MRI CAs in water (solid line) and 4.5% HSA (dashed line) as a function of [Gd].

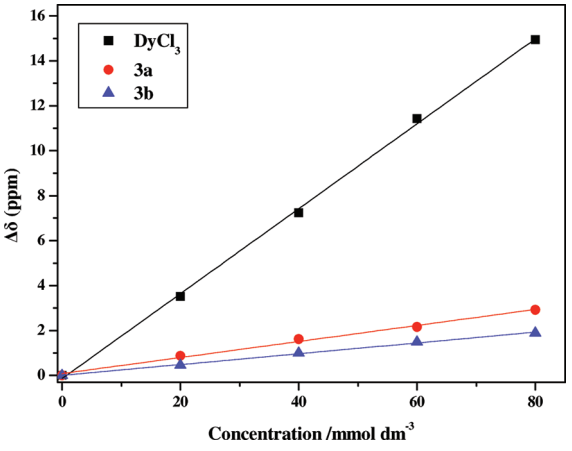


**Figure 7.** Plots of the Dy(III)-induced water $^{17}O$ shifts as function of [Dy].

ions.[31] The figure shows little changes in the evolution rate with **2** compared with clinically available Gd-DTPA analogues.

Although qulitative, the plot of $R_1^P(t)/R_1^P(0)$ as a function of time should provide reliable information about the biostability of **2**. We have thus performed the traditional HPLC measurement for the purpose of consistency.[25] The stability assay on **2b** was conducted by monitoring the signals from a UV absorbance


dx.doi.org/10.1021/jm2002052 |J. Med. Chem. 2011, 54, 5385–5394

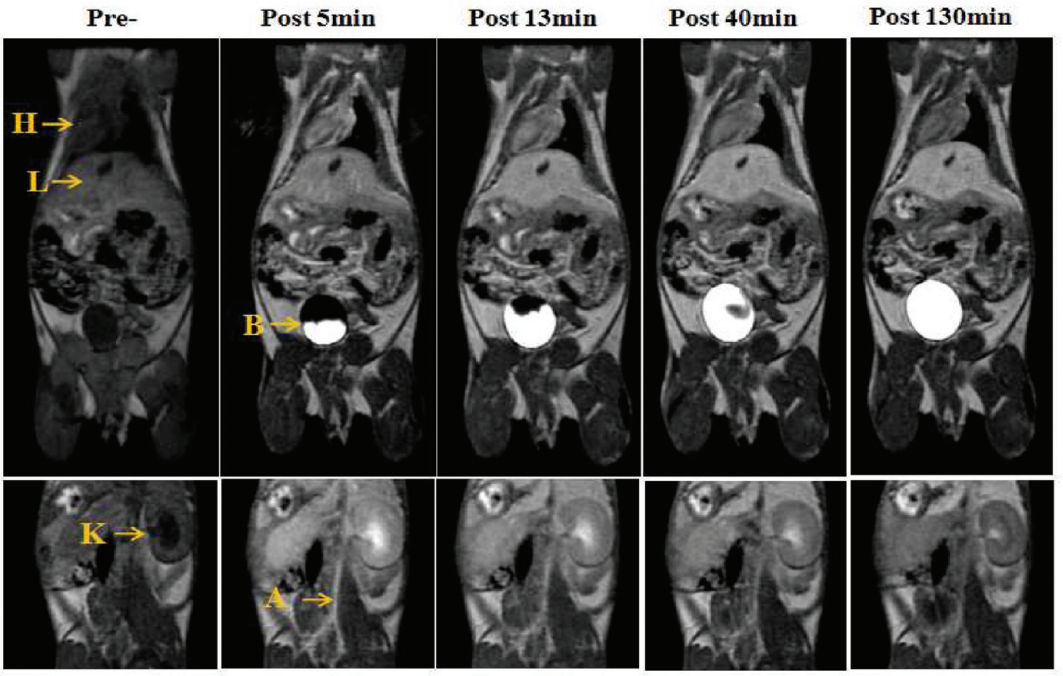


**Figure 8.** In vivo MR coronal images of mice obtained with **2b** (0.1 mmol/kg): H, heart; L, liver; K, kidney; B, bladder; A, abdominal aorta.

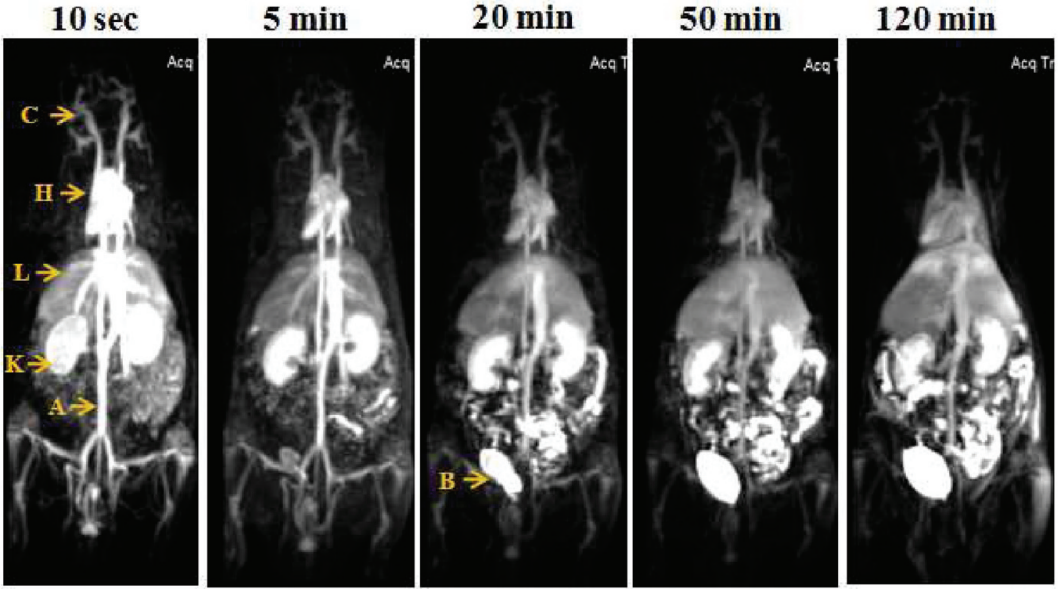


**Figure 9.** In vivo MR coronal maximum intensity projection images of mice obtained by tail vein injection with **2b** (0.1 mmol/kg): C, carotid artery; H, heart; L, liver; K, kidney; B, bladder; A, abdominal aorta.

detector at 240 nm on the HPLC system for an extended period of time. Figure 3 shows the HPLC spectra of **2b** and serum as reference standards. Figure 4 shows that **2b** remains stable enough in human serum for as long as 15 days. Figure 5 shows quantitatively the decrease in the peak area (%) of the spectrum as a function of time. Very little decrease (as low as 5%) is observed within the first 6 days. Even after 15 days, overall decrease was as low as 14%.

**Relaxivity.** Table 2 summarizes $R_1$ relaxivity for **2** along with those for Gd-DTPA and MS-325 for comparative purpose. It is remarkable that **2** shows the highest $R_1$ relaxivities among those examined for comparison both in water and in blood. Even more remarkable is the observation that not only the same relaxivity of **2** reaches almost twice as high as that of MS-325, a well-known MRI BPCA, but also the $R_1/R_2$ value (=0.65) for **2a** is higher than that (=0.51) for MS-325.

A slow tumbling motion (longer rotational correlation time, $\tau_R$) due to the formation of a sterically strained ring by the biphenyl unit might have played a certain role in such high relaxivities exhibited by **2**. The relaxivity increase in the blood further demonstrates the role of the aromatic ring that may be

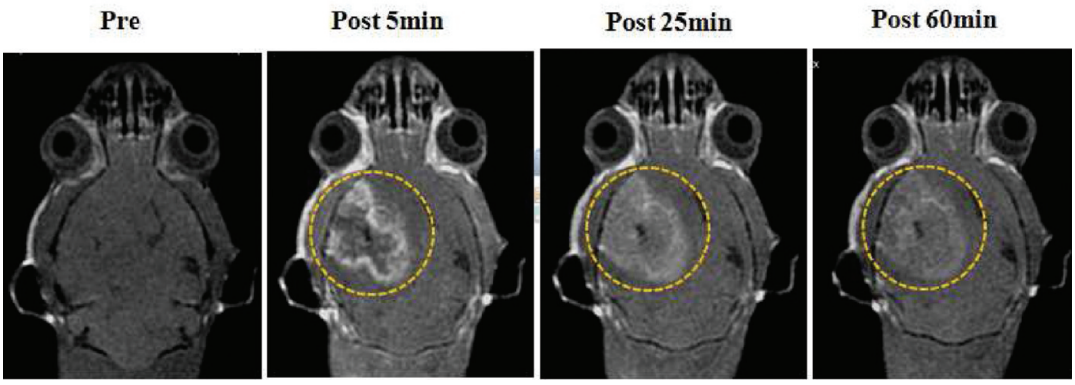


**Figure 10.** In vivo MR coronal images of brain tumor (C6-glyoma cell) obtained with **2b** (0.1 mmol/kg).

involved in the lipophilic interaction with HSA. Figure 6 provides solid evidence for the presence of such an interaction. In HSA solution, the relaxation rates are significantly enhanced compared with those in pure water. For example, the paramagnetic relaxation rate of a solution containing **2** (1 mM) and HSA (4.5%, 0.67 mM) is 3 times as high as that in pure water. On the other hand, little relaxivity increase is observed with either Gd-EOB-DTPA or Gd-BOPTA, well-known BPCAs with liver specificity.

Finally, the most characteristic feature of **2** compared with MS-325, EOB-DTPA, and Gd-BOPTA is that the former is neutral in charge and therefore, unlike the latter, should exhibit no electrostatic interaction. As stated earlier, the electrostatic interaction between the negatively charged chelate in Gd chelate and the positively charged protein moiety is known to make an additional contribution to the relaxivity increase.[32] It is interesting, therefore, to note such high relaxivity with **2** even in the absence of such an electrostatic interaction.

**Dysprosium-Induced Water $^{17}O$ Shifts.** Figure 7 shows the shift of the water $^{17}O$ NMR signal to lower frequencies on addition of **3** compared to $DyCl_3$. As mentioned earlier, the slope of each plot is linearly proportional to the hydration number ($q$), and hydration numbers ($q$) for **3a** and **3b** are found to be 1.16 and 1.79, respectively (see Experimental Section for calculation). These observations may justify our hypothesis made above in connection with such high relaxivities exhibited by **3**. In other words, a macrocyclic ring conformation of **3**, rather than the hydration number, seems to play a more prominent role in their relaxivities.

**In Vivo MR Imaging.** Figure 8 shows the coronal $T_1$-weighted images of 6-week-old male mice, ICR for **2b**, and Figure 9 shows the coronal $T_1$-weighted angiography images of 10-week-old male SD rats as a function of time. A strong blood-pool effect is observed from the signal enhancement in both heart and abdominal aorta. Signal enhancement is observed in various arteries and vessels and lasts as long as 120 min after injection as demonstrated in Figure 9. Renal excretion is observed 20 min after injection as evidenced by enhancement in kidneys and bladder. The CNR profiles shown in Figure S2 provide concurring observations made in connection with Figures 8 and 9.[34,35] Even more striking, **2b** is able to enhance the brain tumor for as long as an hour, which is a rare example of ordinary ECF MRI CAs exhibiting such behavior (Figure 10). For instance, we have provided supporting evidence in Figure S3 showing the CNR profiles obtained with **2b** to be much greater during the early stage of injection than those with Gd-DOTA, a well-known ECF CA. The long circulation time and the subsequent high concentration in blood might have caused such enhancement in brain tumor, and as such a noncovalent interaction of biphenyl with HSA seems to play a certain role in the long retention time in blood.

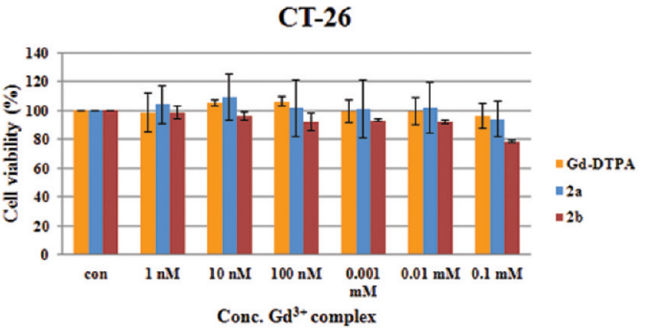


**Figure 11.** Cell viability for **2** and Gd-DTPA.

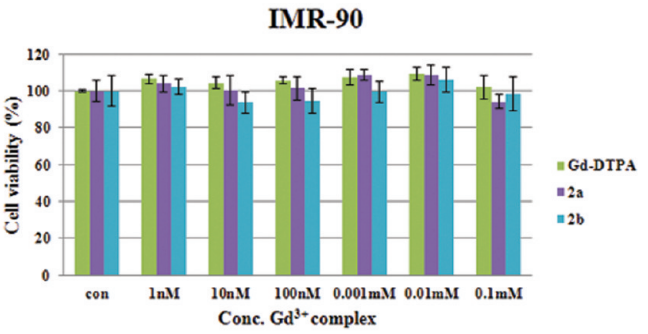


**Figure 12.** Cell viability for **2** and Gd-DTPA-BMA.

**In Vitro Cell Toxicity.** Figures 11 and 12 show the cytotoxicity tests performed on CT-26 mouse colon carcinoma cell and IMR-90 human embryonic lung fibroblasts with **2**. Cytotoxicity of the present series compares well with that of Gd-DTPA and Gd-DTPA-BMA. When the comparison is made between **2a** and **2b**, the former shows a little lower cytotoxicity. A related observation is that cell viability for **2b** decreases gradually with an increase in its concentration.

## CONCLUSION

The reaction of 2,2′-diaminobiphenyls with DTPA-bis(anhydride) yielded corresponding macrocyclic DTPA-bis(amides)


dx.doi.org/10.1021/jm2002052 |J. Med. Chem. 2011, 54, 5385–5394

(**2a**,**b**) rather than acyclic, oligomeric analogues. They form on reaction with $Gd(OAc)_3$ corresponding Gd complexes of the type $[Gd(\mathbf{L})(H_2O)]\cdot xH_2O$ (**2a**,**b**; **L** = **1a**,**b**). Pharmacokinetic inertness of **2** compares well with that of analogous Gd-DTPA MRI CAs currently in use. The $R_1$ relaxivity reaches as high as 10.9 $mM^{-1}$ $s^{-1}$. This value is approximately 3 times as high as that of Gd-DOTA ($R_1$ = 3.7 $mM^{-1}$ $s^{-1}$). The $R_1$ relaxivity in HSA is 37.2 $mM^{-1}$ $s^{-1}$, which is almost twice as high as that of MS-325, a leading BPCA, demonstrating a strong blood pool effect. The in vivo MR images of mice obtained with **2b** are coherent, showing strong signal enhancement in heart, abdominal aorta, and small vessels. Further, even the brain tumor is vividly enhanced for an extended period of time. The structural uniqueness of **2** is that it is neutral in charge and thus makes no resort to electrostatic interaction, supposedly one of the essential factors for the blood-pool effect.

## ■ ASSOCIATED CONTENT

**Supporting Information.** Kinetic inertness fitting data, in vivo CNR profiles, and osmolality data; zipped file containing a video of MR of mouse in avi format. This material is available free of charge via the Internet at http://pubs.acs.org.

## ■ AUTHOR INFORMATION

### Corresponding Author

*For Y.C.: phone, (+)82-53-420-5471; e-mail, ychang@knu.ac.kr. For T.-J.K.: phone, (+)82-53-950-5587; fax, (+)82-53-950-6594; e-mail, tjkim@knu.ac.kr.

## ■ ACKNOWLEDGMENT

T.-J.K. and Y.C. gratefully acknowledge NRF (Grant No. 2010-0024143) and NRF (Grant No. 2009-0072413), respectively, for financial support. KBSI, Daegu branch, is also acknowledged for the mass spectral measurements.

## ■ ABBREVIATIONS USED

DTPA, diethylentriamine-*N*,*N*,*N*′,*N*″,*N*″-pentaacetic acid; MRI, magnetic resonance imaging; BPCA, blood-pool contrast agent; CA, contrast agent; DOTA, 1,4,7,10-tetraazacyclododecane-*N*,*N*′,*N*″,*N*‴-1,4,7,10-tetraacetic acid; MS-325, (trisodium {(2-(*R*)-[(4,4-diphenylcyclohexyl)phosphonooxymethyl]diethylenetriaminepentaacetato)(aquo)gadolinium(III)}; ECF, extracellular fluid; HSA, human serum albumin; TI, inversion time; TE, echo time; TR, repetition time; ICR, Institute of Cancer Research; SD, Sprague—Dawley; NEX, number of acquisitions; ROI, region of interest; TMS, tetramethylsilane; DTPA-BMA, *N*,*N*″-bis(methylamide) of DTPA; EOB-DTPA, *S*-[4-(4-ethoxybenzyl)-3,6,9-tris(carboxylatomethyl)-3,6,9-triazaundecanedioic acid; BOPTA, 4-carboxy-5,8,11-tris(carboxylmethyl)-l-pheny1-2-oxa-5,8,11- riazatridecan-13-oic acid

## ■ REFERENCES

(1) Caravan, P. Strategies for increasing the sensitivity of gadolinium based MRI contrast agents. *Chem. Soc. Rev.* **2006**, *35* (6), 512–523.

(2) Caravan, P.; Ellison, J. J.; McMurry, T. J.; Lauffer, R. B. Gadolinium(III) chelates as MRI contrast agents: structure, dynamics, and applications. *Chem. Rev.* **1999**, *99* (9), 2293–2352.

(3) Kobayashi, H.; Sato, N.; Hiraga, A.; Saga, T.; Nakamoto, Y.; Ueda, H.; Konishi, J.; Togashi, K.; Brechbiel, M. W. 3D-micro-MR angiography of mice using macromolecular MR contrast agents with polyamidoamine dendrimer core with references to their pharmacokinetic properties. *Magn. Reson. Med.* **2001**, *45* (3), 454–460.

(4) Ayyagari, A. L.; Zhang, X. D.; Ghaghada, K. B.; Annapragada, A.; Hu, X. P.; Bellamkonda, R. V. Long-circulating liposomal contrast agents for magnetic resonance imaging. *Magn. Reson. Med.* **2006**, *55* (5), 1023–1029.

(5) Schwickert, H. C.; Stiskal, M.; Vandijke, C. F.; Roberts, T. P.; Mann, J. S.; Demsar, F.; Brasch, R. C. Tumor angiography using high resolution 3D MRI: comparison of Gd-DTPA and a macromolecular blood pool contrast agent. *Acad. Radiol.* **1995**, *2* (10), 851–858.

(6) Lauffer, R. B.; Parmelee, D. J.; Dunham, S. U.; Ouellet, H. S.; Dolan, R. P.; Witte, S.; McMurry, T. J.; Walovitch, R. C. MS-325: albumin-targeted contrast agent for MR angiography. *Radiology (Oak Brook, IL, U. S.)* **1998**, *207* (2), 529–538.

(7) Cavagna, F. M.; Lorusso, V.; Anelli, P. L.; Maggioni, F.; de Haën, C. Preclinical profile and clinical potential of gadocoletic acid trisodium salt (B22956/1), a new intravascular contrast medium for MRI. *Acad. Radiol.* **2002**, *9*, S491–S494.

(8) Preda, A.; Novikov, V.; Möglich, M.; Turetschek, M. K.; Shames, D. M.; Brasch, R. C.; Cavagna, F. M.; Roberts, T. P. L. MRI monitoring of avastin antiangiogenesis therapy using B22956/1, a new blood pool contrast agent, in an experimental model of human cancer. *J. Magn. Reson. Imaging* **2004**, *20* (5), 865–873.

(9) Merbach, A. E.; Tóth, E. *The Chemistry of Contrast Agents in Medial Magnetic Resonance Imaging*; Wiley-VCH: Chichester, U.K., 2001.

(10) Aime, S.; Botta, M.; Crich, S. G.; Giovenzana, G.; Palmisano, G.; Sisti, M. Novel paramagnetic macromolecular complexes derived from the linkage of a macrocyclic Gd(III) complex to polyamino acids through a squaric acid moiety. *Bioconjugate Chem.* **1999**, *10* (2), 192–199.

(11) Curtet, C.; Maton, F.; Havet, T.; Slinkin, M.; Mishra, A.; Chatal., J. F.; Muller, R. N. Polylysine-Gd-DTPAn and polylysine-Gd-DOTAn coupled to anti-CEA F(ab′)2 fragments as potential immunocontrast agents. Relaxometry, biodistribution, and magnetic resonance imaging in nude mice grafted with human colorectal carcinoma. *Invest. Radiol.* **1998**, *33* (10), 752–761.

(12) Lokling, K. E.; Fossheim, S. L.; Skurtveit, R.; Bjornerud, A.; Klaveness, J. pH-sensitive paramagnetic liposomes as MRI contrast agents: in vitro feasibility studies. *Magn. Reson. Imaging* **2001**, *19* (5), 731–738.

(13) Jung, C. W.; Jacobs, P. Physical and chemical properties of superparamagnetic iron oxide MR contrast agents: ferumoxides, ferumoxtran, ferumoxsil. *Magn. Reson. Imaging* **1995**, *13* (5), 661–674.

(14) Taupitz, M.; Schnorr, J.; Abramjuk, C.; Wagner, S.; Pilgrimm, H.; Hünigen, H.; Hamm, B. New generation of monomer-stabilized very small superparamagnetic iron oxide particles (VSOP) as contrast medium for MR angiography: preclinical results in rats and rabbits. *J. Magn. Reson. Imaging* **2000**, *12* (6), 905–911.

(15) Mornet, S.; Vasseur, S.; Grasset, F.; Duguet, E. Magnetic nanoparticle design for medical diagnosis and therapy. *J. Mater. Chem.* **2004**, *14* (14), 2161–2175.

(16) Avedano, S.; Tei, L.; Lombardi, A.; Giovenzana, G. B.; Aime, S.; Longo, D.; Botta, M. Maximizing the relaxivity of HSA-bound gadolinium complexes by simultaneous optimization of rotation and water exchange. *Chem. Commun.* **2007**, *45*, 4726–4728.

(17) Henrotte, V.; Elst, L. V.; Laurent, S.; Muller, R. N. Comprehensive investigation of non-covalent binding of MRI contrast agents with human serum albumin. *J. Biol. Inorg. Chem.* **2007**, *12* (6), 929–937.

(18) (a) Kim, H.-K.; Jung, H.-Y.; Park, J.-A.; Huh, M.-I.; Jung, J.-C.; Chang, Y.; Kim, T.-J. Gold nanoparticles coated with gadolinium-DTPA-bisamide conjugate of penicillamine (Au@GdL) as a T1-weighted blood pool contrast agent. *J. Mater. Chem.* **2010**, *20* (26), 5411–5417. (b) Kim, H.-K.; Park, J.-A.; Kim, K. M.; Md., M. S.; Kang, D.-S.; Lee, J.; Chang, Y.; Kim, T.-J. Gd-complexes of macrocyclic DTPA conjugates of 1,1′-bis(amino)ferrocenes as high relaxivity MRI blood-pool contrast agents (BPCAs). *Chem. Commun.* **2010**, *46*

(44), 8442–8444. (c) Gu, S.; Kim, H.-K.; Lee, G. H.; Kang, B.-S.; Chang, Y.; Kim, T.-J. Gd-Complexes of 1,4,7,10-tetraazacyclododecane-*N*,*N*′,*N*″,*N*‴-1,4,7,10-tetraacetic acid (DOTA) conjugates of tranexamates as a new class of blood-pool magnetic resonance imaging contrast agents. *J. Med. Chem.* **2011**, *54* (1), 143–152.

(19) Eckelman, W. C.; Karesh, S. M.; Reba, R. C. New compounds: fatty acid and long chain hydrocarbon derivatives containing a strong chelating agent. *J. Pharm. Sci.* **1975**, *64* (4), 704–706.

(20) Ol'khovik, V. K.; Pap, A. A.; Vasilevskii, V. A.; Galinovskii, N. A.; Tereshko, S. N. Synthesis and properties of luminophores derived from fluorinated biphenyls. *Russ. J. Chem.* **2008**, *44* (8), 1172–1179.

(21) Laurent, S.; Elst, L. V.; Copoix, F.; Muller, R. N. Stability of MRI paramagnetic contrast media. A proton relaxometric protocol for transmetallation assessment. *Invest. Radiol.* **2001**, *36* (2), 115–122.

(22) Alpoim, M. C.; Urbano, A. M.; Geraldes, C. F. G. C.; Peters, J. A. Determination of the number of molecules in lanthanide(III) polyaminocarboxylate complexes. *Dalton Trans.* **1992**, *3*, 463–467.

(23) Fonchy, E.; Lahrech, H.; François-Joubert, a; Dupeyre, R.; Benderbous, S.; Corot, C.; Farion, R.; Rubin, C.; Décorps, M.; Rémy, C. A new gadolinium-based contrast agent for magnetic resonance imaging of branin tumors: kinetic study on a C6 rat glioma model. *J. Magn. Reson. Imaging* **2001**, *14* (2), 97–105.

(24) Frenzel, T.; Lengsfeld, P.; Schirmer, H.; Hütter, J.; Weinmann, H.-J. Stability of gadolinium-based magnetic resonance imaging contrast agents in human serum at 37 degrees C. *Invest. Radiol.* **2008**, *43* (12), 817–828.

(25) Zhang, Z.; Liang, K.; Bloch, S.; Berezin, M.; Achilefu, S. Monomolecular multimodal fluorescence-radioisotope imaging agents. *Bioconjugate Chem.* **2005**, *16* (5), 1232–1239.

(26) Puttagunta, N. R.; Gibby, W. A.; Puttagunta, V. L. Comparative transmetallation kinetics and thermodynamic stability of gadolinium-DTPA bis-glucosamide and other magnetic resonance imaging contrast media. *Invest. Radiol.* **1996**, *31* (10), 619–624.

(27) Corot, C.; Idee, J. M.; Hentsch, A. M.; Santus, R.; Mallet, C.; Goulas, V.; Bonnemain, B.; Meyer, D. Structure−activity relationship of macrocyclic and linear gadolinium chelates: investigation of transmetallation effect on the zinc-dependent metallopeptidase angiotensin-converting enzyme. *J. Magn. Reson. Imaging* **1998**, *8* (3), 695–702.

(28) Corot, C.; Hentsch, A.-M.; Curtelin, L. Interaction of gadolinium complexes with metal-dependent biological systems. *Invest. Radiol.* **1994**, *29* (Suppl. 2), S164–S167.

(29) Laurent, S.; Vander Elst, L.; Copoix, F.; Muller, R. N. Stability of MRI paramagnetic contrast media: a proton relaxometric protocol for transmetallation assessment. *Invest. Radiol.* **2001**, *36* (2), 115–122.

(30) Laurent, S.; Vander Elst, L.; Muller, R. N. Comparative study of the physicochemical properties of six clinical low molecular weight gadolinium contrast agents. *Contrast Media Mol. Imaging* **2006**, *1* (3), 128–137.

(31) Lauffer, R. B. Pramagnetic metal complex as water proton relaxation agents for NMR imaging: theory and design. *Chem. Rev.* **1987**, *87* (5), 901–972.

(32) Chan, K. W.-Y.; Wong, W.-T. Small molecular gadolinium(III) complexes as MRI contrast agents for diagnostic imaging. *Coord. Chem. Rev.* **2007**, *251* (17−20), 2428–2451.

(33) Bremerich, J.; Bilecen, D.; Reimer, P. MR angiography with blood pool contrast agents. *Eur. Radiol.* **2007**, *17* (12), 3017–3024.

(34) Kiryu, S.; Inoue, Y.; Watanabe, M.; Izawa, K.; Shimada, M.; Tojo, A.; Yoshikawa, K.; Ohtomo, K. Evaluation of gadoxetate disodium as a contrast agent for mouse liver imaging: comparison with gadobenate dimeglumine. *Magn. Reson. Imaging* **2009**, *27* (1), 101–107.

(35) Schima, W.; Petersein, J.; Hahn, P. F.; Harisinghani, M.; Halpern, E.; Saini, S. Contrast-enhanced MR imaging of the liver: comparison between Gd-BOPTA and mangafodipir. *J. Magn. Reson. Imaging* **1997**, *7* (1), 130–135.